Journal of Sound and Vibration 332 (2013) 7243–7256

Contents lists available at ScienceDirect

Journal of Sound and Vibration

journal homepage: www.elsevier.com/locate/jsvi

The propagation of coupled Lamb waves in multilayered arbitrary anisotropic composite laminates

He Cunfu*, Liu Hongye, Liu Zenghua, Wu Bin

College of Mechanical Engineering and Applied Electronics Technology, Beijing University of Technology, Pingleyuan 100, Chaoyang District, Beijing 100124, PR China

ARTICLE INFO

Article history:
Received 1 December 2012
Received in revised form
2 August 2013
Accepted 19 August 2013
Handling Editor: G. Degrande
Available online 17 September 2013

ABSTRACT

Based on linear three-dimensional elasticity theory, the wave equations of coupled Lamb waves in multilayered arbitrary anisotropic composite laminates are derived using a Legendre orthogonal polynomial approach. The elastodynamic solution for the propagation of coupled Lamb waves in composite plates is also presented to determine the characteristics of coupled Lamb waves. To verify the applicability and validity of the method, two cases of bi-layered plates formed with isotropic components and anisotropic components, respectively, are primarily manipulated for comparison with earlier known results. Next, the dispersion curves, displacements and stress distributions of Lamb waves in multilayered anisotropic laminates are calculated. The effects of coupling and fiber orientation on the characteristics of the Lamb waves are illustrated. The potential usefulness of the fundamental modes of the coupled Lamb waves is discussed in detail.

1. Introduction

In recent years, the use of composite materials in many advanced industries has increased rapidly due to the excellent material properties of composites, which include relatively high modulus values, high specific strength and outstanding designability characteristics. The advantages of composite materials allow them to be tailored to many different engineering applications and work environments, such as parts used in aircraft structures, civil constructions and automobiles. However, due to the unexpected complications associated with the exterior impacts incurred during complex manufacturing processes and the inevitable deterioration of material properties during in-service applications, composite materials also have a high probability of defect generation and growth. To achieve non-destructive testing and aging controls for composite materials, it is critical that we develop a reliable non-destructive evaluation method. Lamb wave technology is considered a promising candidate because of its potential for implementation in applications of structural health monitoring. The effective use of Lamb wave technology for such a purpose largely depends on developing a good understanding of the mechanics of wave propagation in composite laminates.

The characteristic analysis of Lamb waves in layered structures has received significant attention from many researchers, with much work reported on the problem of wave propagation in layered structures. Matrix techniques have been popular for the modeling of ultrasonic wave propagation in multilayered plates in recent decades. Nayfeh [1–3] developed a transfer matrix technique to acquire the dispersion curves of Lamb waves in laminates and gave a comprehensive theoretical analysis of Lamb wave propagation in multilayered anisotropic media. Hosten et al. [4] modified the expression of a transfer

* Corresponding author. Tel.: +8610 6739 1938.
E-mail addresses: hecunfu@bjut.edu.cn (H. Cunfu), hongye@emails.bjut.edu.cn (L. Hongye).

0022-460X/$ - see front matter © 2013 Elsevier Ltd. All rights reserved.
http://dx.doi.org/10.1016/j.jsv.2013.08.035

matrix for one elementary ply, taking the heterogeneity of the generated Lamb wave modes at interfaces between the absorbing media into consideration, introducing anisotropic attenuation into the formulation of the transfer matrix by using an adaptation of the well-known Thomson–Haskell method. Potel et al. [5] studied wave propagation in an anisotropic periodic multilayered medium using the Thomson–Haskell method and gave physical explanations for a layer composed of a monoclinic crystal system medium. Ogilvy [6] combined plane wave solutions to analyze the behavior of Lamb waves in layered anisotropic plates; these solutions were suitable for either perfect adhesion or slip–bond interface conditions. Although the transfer matrix method is very compact in form and can be readily implemented in new situations, it suffers from an important problem: the solution becomes unstable when the propagation sensitive parameter "*fd*" (the product of frequency and plate thickness) is very large.

In parallel with the transfer matrix method, an alternative and significantly different assembled matrix method, known as the global matrix method, was proposed by Knopoff [7], in which a large single matrix is assembled and all of the equations possess terms for all of the layers. Lowe [8] described the global matrix method in sufficient detail, modifying the spatial origins of the bulk waves in each layer; the author found the method to be perfectly reliable when seeding the root-finding algorithm for the modal solution calculation. The global matrix method incorporates the material damping and leaky mode developments and does not suffer from numerical instability; however, the approach may require long computing times when either the layer number or the matrix size is very large.

Additionally, as a discretization technique using the variation principle to find a stable solution to boundary value problems, the finite element method is now widely used in the analysis of Lamb wave propagation and the interaction of Lamb waves with different types of defects. Hosten et al. [9] calculated the stress and displacement distributions in plates made of anisotropic viscoelastic materials using a finite element code in a stationary state and investigated the problem of Lamb wave diffraction by defects, including notches and delamination. Ng et al. [10] analyzed the scattering of the fundamental anti-symmetric A_0 mode at a delamination defect in a quasi-isotropic composite plate by using the three-dimensional finite element method. Further, experimental measurements were performed to give physical insight into the scattering phenomena and verified the simulation results. Al-Qahtani et al. [11] studied the generation of transient Lamb waves in an anisotropic infinite plate using a semi-analytical finite element method. The efficiency of the finite element method has been extensively studied in terms of the characteristic analysis of wave propagation in multilayered anisotropic structures. However, there are several obvious disadvantages associated with finite element methods, including the significant number of mesh elements that is usually required and the cost of calculation, which is generally too high for the simulation of many common structures.

To analyze the behavior of wave propagation in more complex materials, some researchers have resorted to mathematically approximate or asymptotic approaches. Li et al. [12] investigated Love wave propagation in a layered functionally graded piezoelectric structure and solved the electromechanical field differential equations using the WKB method, which was first proposed by Wentzel, Kramers, Brillouin and Jeffreys in the mid-1920s. Liu et al. [13] used the WKB method to obtain the phase velocity equations of Love waves for both electrical open and short circuit cases on free surfaces in functionally graded layered piezoelectric structures. Lefebvre et al. [14] developed a Legendre polynomial approach with position-dependent elastic constants to study the propagation of Lamb waves in continuous functionally graded plates. The key aspect of this approach is its theoretical development from an orthonormal basis set for the expansion of the field quantities. As discussed in some works [14–17], the significant advantage of this method is that the tedious iterative two-variable search can be avoided when the usual solution necessitates an iterative search procedure to calculate the complex roots of a frequency equation with the goal of acquiring the wave velocity. Compared to other methods that do not require an iterative search for the solutions, the assumed solution form of the field components in this approach is expressed by a linear combination of orthonormal functions, which reduces the mathematical issue to an eigenvalue problem. By means of the reduction, eigenvalues yield the guided wave velocities, and eigenvectors enable field profiles to be calculated easily. However, due to the introduction of position-dependent elastic constants, this method is readily extended to more complex structures, for which the inhomogeneity can be parameterized as a function of the position variable. As a result, it is no longer necessary to approximate the material as successive layers of homogeneous materials whose properties vary slowly from layer to layer and whose thickness is small compared to the wavelength. Further, convergent results can be obtained with very low truncation numbers and larger values of the frequency–thickness product are allowed relative to that of the other commonly used methods [15,16]. Additionally, with this method, it is easy to incorporate boundary conditions by applying the rectangular window function [17]. Anisotropy can be handled in a straightforward manner, and all modes are easily obtained. Wu et al. [18] used this approach to investigate the influences of piezoelectricity and piezomagnetism on the dispersion properties of wave propagation in inhomogeneous magneto–electro-elastic plates. Then, Yu et al. [19–21] extended this approach to investigate wave propagation in other relevant structures with more complex material parameters.

Based on a review of previous literature, it can be observed that the propagation of Lamb waves in multilayered plates, with individual lamina consisting of isotropic or orthogonal components, has received significant attention, although few reports have involved studies of coupled Lamb wave propagation based on a mathematically approximate approach. In non-destructive testing or structural health monitoring, the condition of Lamb waves propagating along a non-principal direction is actually common due to the irregular distribution of sensor placements, complicated anisotropy and different observation directions [22–24]. In the present paper, our attention is mainly focused on the derivation and analysis of coupled Lamb wave equations for multilayered arbitrary anisotropic composite laminates using the Legendre orthogonal polynomial approach. Based on linear three-dimensional elasticity theory, the relevant formulations are first derived, and two cases,

a bi-layered isotropic plate and a bi-layered composite laminate, are subsequently given for comparison against known results. The dispersion curves, displacements and stress distributions of the fundamental Lamb wave modes are also illustrated in detail. The influences of fiber orientation on the characteristic behaviors of the coupled Lamb waves are subsequently discussed.

2. Mathematics and problem formulation

Consider a multilayered anisotropic plate that is infinite in the horizontal direction and has thickness h_N, as shown in Fig. 1, where the composite media occupies the region $0 \le x_3 \le h_N$. The horizontal x_1-x_2 plane of the Cartesian coordinates is on the top surface of the multilayered anisotropic plate, and o is the origin of the Cartesian coordinates. We assume that the x_1-axis is in the direction of wave propagation and that the x_3-axis is perpendicular to the outer surfaces. Each lamina is arbitrary anisotropic, and the elastic medium of the individual component is characterized by constant mass density ρ and elastic constant c. Here, the $o-x_1x_2x_3$ coordinate system is defined as the global coordinate system. If the material tensors are defined in terms of the crystallographic axes, their components must be first transformed into equivalent global tensors with the goal of matching the global coordinate system, as depicted in Fig. 1.

For arbitrary anisotropic material, the generalized Hooke's law, implying the stress–strain relation, can be written in the following form [25]:

$$\begin{Bmatrix} \sigma_{11} \\ \sigma_{22} \\ \sigma_{33} \\ \sigma_{23} \\ \sigma_{13} \\ \sigma_{12} \end{Bmatrix} = \begin{bmatrix} c_{11} & c_{12} & c_{13} & c_{14} & c_{15} & c_{16} \\ & c_{22} & c_{23} & c_{24} & c_{25} & c_{26} \\ & & c_{33} & c_{34} & c_{35} & c_{36} \\ & \text{symmetry} & & c_{44} & c_{45} & c_{46} \\ & & & & c_{55} & c_{56} \\ & & & & & c_{66} \end{bmatrix} \begin{Bmatrix} \varepsilon_{11} \\ \varepsilon_{22} \\ \varepsilon_{33} \\ 2\varepsilon_{23} \\ 2\varepsilon_{13} \\ 2\varepsilon_{12} \end{Bmatrix} \tag{1}$$

where c_{kl} $(k,l=1,2,3,4,5,6)$ identifies the stiffness matrix and represents the elastic constant of the anisotropic medium. σ_{ij} and ε_{ij} are defined as the stress and strain tensors, respectively. The subscripts i and j take on the values of $1,2,3$.

Under the assumption of small deformations, the relationship between the strain and displacement in terms of the Cartesian coordinate system can be expressed as

$$\varepsilon_{11}=\frac{\partial u_1}{\partial x_1}, \quad \varepsilon_{22}=\frac{\partial u_2}{\partial x_2}, \quad \varepsilon_{33}=\frac{\partial u_3}{\partial x_3},$$
$$\varepsilon_{23}=\frac{1}{2}\left(\frac{\partial u_2}{\partial x_3}+\frac{\partial u_3}{\partial x_2}\right), \quad \varepsilon_{13}=\frac{1}{2}\left(\frac{\partial u_1}{\partial x_3}+\frac{\partial u_3}{\partial x_1}\right), \quad \varepsilon_{12}=\frac{1}{2}\left(\frac{\partial u_1}{\partial x_2}+\frac{\partial u_2}{\partial x_1}\right) \tag{2}$$

where u_i stand for the elastic displacements.

In Cartesian coordinates, the field equations governing wave propagation in a multilayered anisotropic plate are given by

$$\begin{aligned} \frac{\partial \sigma_{11}}{\partial x_1}+\frac{\partial \sigma_{12}}{\partial x_2}+\frac{\partial \sigma_{13}}{\partial x_3}&=\rho\frac{\partial^2 u_1}{\partial t^2} \\ \frac{\partial \sigma_{21}}{\partial x_1}+\frac{\partial \sigma_{22}}{\partial x_2}+\frac{\partial \sigma_{23}}{\partial x_3}&=\rho\frac{\partial^2 u_2}{\partial t^2} \\ \frac{\partial \sigma_{31}}{\partial x_1}+\frac{\partial \sigma_{32}}{\partial x_2}+\frac{\partial \sigma_{33}}{\partial x_3}&=\rho\frac{\partial^2 u_3}{\partial t^2} \end{aligned} \tag{3}$$

where ρ is the mass density of the material.

Considering the boundary conditions, the rectangular window function $\pi_{h_0,h_N}(x_3)$ can be introduced by

$$\pi_{h_0,h_N}(x_3)=\begin{cases} 1, & h_0 \le x_3 \le h_N \\ 0, & \text{elsewhere} \end{cases}$$

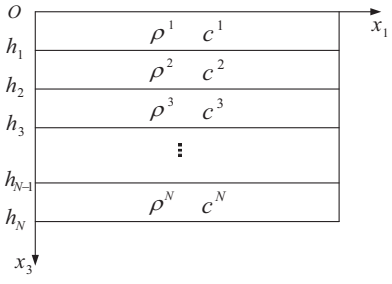

Fig. 1. A schematic diagram of a multilayered anisotropic plate, showing the coordinate system.

Here, N is the number of layers, and $h_0=0$. By introducing the rectangular window function, the stress-free boundary conditions ($\sigma_{33}=\sigma_{13}=\sigma_{23}=0$ at $x_3=0, x_3=h_N$) are automatically satisfied [15,16]. The constitutive relations can be rewritten as follows:

$$\begin{aligned}
\sigma_{11} &= (c_{11}\varepsilon_{11}+c_{12}\varepsilon_{22}+c_{13}\varepsilon_{33}+2c_{14}\varepsilon_{23}+2c_{15}\varepsilon_{13}+2c_{16}\varepsilon_{12})\pi_{0,h_N}(x_3)\\
\sigma_{22} &= (c_{12}\varepsilon_{11}+c_{22}\varepsilon_{22}+c_{23}\varepsilon_{33}+2c_{24}\varepsilon_{23}+2c_{25}\varepsilon_{13}+2c_{26}\varepsilon_{12})\pi_{0,h_N}(x_3)\\
\sigma_{33} &= (c_{13}\varepsilon_{11}+c_{23}\varepsilon_{22}+c_{33}\varepsilon_{33}+2c_{34}\varepsilon_{23}+2c_{35}\varepsilon_{13}+2c_{36}\varepsilon_{12})\pi_{0,h_N}(x_3)\\
\sigma_{23} &= (c_{14}\varepsilon_{11}+c_{24}\varepsilon_{22}+c_{34}\varepsilon_{33}+2c_{44}\varepsilon_{23}+2c_{45}\varepsilon_{13}+2c_{46}\varepsilon_{12})\pi_{0,h_N}(x_3)\\
\sigma_{13} &= (c_{15}\varepsilon_{11}+c_{25}\varepsilon_{22}+c_{35}\varepsilon_{33}+2c_{45}\varepsilon_{23}+2c_{55}\varepsilon_{13}+2c_{56}\varepsilon_{12})\pi_{0,h_N}(x_3)\\
\sigma_{12} &= (c_{16}\varepsilon_{11}+c_{26}\varepsilon_{22}+c_{36}\varepsilon_{33}+2c_{46}\varepsilon_{23}+2c_{56}\varepsilon_{13}+2c_{66}\varepsilon_{12})\pi_{0,h_N}(x_3)
\end{aligned} \tag{4}$$

Because the mechanical properties of the multilayered anisotropic laminates vary in the thickness direction, the elastic constant of the media is a function of x_3, so it can be compactly expressed as

$$c_{kl}=\sum_{n=1}^{N} c_{kl}^{n}\pi_{h_{n-1},h_n}(x_3) \tag{5a}$$

where c_{kl}^{n} is the elastic constant c_{kl} in the nth layer. Likewise, the mass density of the laminates can be expressed as

$$\rho=\sum_{n=1}^{N} \rho^{n}\pi_{h_{n-1},h_n}(x_3) \tag{5b}$$

with ρ^n being the mass density in the nth layer of the plates.

For the steady-state solutions of free harmonic wave propagation in the x_1 direction, we assume the displacement components are of the form

$$u_1(x_1,x_2,x_3,t)=\exp[\mathrm{i}(kx_1-\omega t)]U(x_3) \tag{6a}$$

$$u_2(x_1,x_2,x_3,t)=\exp[\mathrm{i}(kx_1-\omega t)]V(x_3) \tag{6b}$$

$$u_3(x_1,x_2,x_3,t)=\exp[\mathrm{i}(kx_1-\omega t)]W(x_3) \tag{6c}$$

where $U(x_3), V(x_3), W(x_3)$ represent the magnitudes of the fields in the x_1, x_2, x_3 directions, respectively. k is the magnitude of the wave vector in the propagation direction, and ω is the angular frequency.

Substituting Eqs. (2, 4–6) into Eq. (3), the governing differential equations in terms of the displacement quantities can be given

$$\begin{aligned}
&c_{55}U''+[(\mathrm{i}k)2c_{15}'+c_{55}]U'+[-k^2c_{11}+(\mathrm{i}k)c_{15}']U+c_{45}V''\\
&+[(\mathrm{i}k)(c_{14}+c_{56})+c_{45}']V'+[-k^2c_{16}+(\mathrm{i}k)c_{56}']V+c_{35}W''\\
&+[(\mathrm{i}k)(c_{13}+c_{55})+c_{35}']W'+[-k^2c_{15}+(\mathrm{i}k)c_{55}']W=-\rho\omega^2U
\end{aligned} \tag{7a}$$

$$\begin{aligned}
&c_{45}U''+[(\mathrm{i}k)(c_{14}+c_{56})+c_{45}']U'+[-k^2c_{16}+(\mathrm{i}k)c_{14}']U+c_{44}V''\\
&+[(\mathrm{i}k)2c_{46}+c_{44}']V'+[-k^2c_{66}+(\mathrm{i}k)c_{46}']V+c_{34}W''\\
&+[(\mathrm{i}k)(c_{36}+c_{45})+c_{34}']W'+[-k^2c_{56}+(\mathrm{i}k)c_{45}']W=-\rho\omega^2V
\end{aligned} \tag{7b}$$

$$\begin{aligned}
&c_{35}U''+[(\mathrm{i}k)(c_{13}+c_{55})+c_{35}']U'+[-k^2c_{15}+(\mathrm{i}k)c_{13}']U+c_{34}V''\\
&+[(\mathrm{i}k)(c_{36}+c_{45})+c_{34}']V'+[-k^2c_{56}+(\mathrm{i}k)c_{36}']V+c_{33}W''\\
&+[(\mathrm{i}k)2c_{35}+c_{33}']W'+[-k^2c_{55}+(\mathrm{i}k)c_{35}']W=-\rho\omega^2W
\end{aligned} \tag{7c}$$

Here, Eqs. (7a), (7b) and (7c) are coupled Lamb wave equations that govern the propagation of Lamb waves in a multilayered arbitrary anisotropic plate. They are different from the cases of the isotropic or orthogonal individual component, in which Eq. (7b) is independent of the other two equations and represents the uncoupled SH waves.

To obtain the solutions of the coupled Lamb wave equations governed by the coupled differential Eqs. (7a), (7b) and (7c), the displacement quantities can be expanded in the Legendre polynomial, which is complete and orthogonal. By "complete," we mean that the polynomial is able to represent any well-behaved (at least, piecewise continuous) function. Hence, the displacement quantities $U(x_3)$, $V(x_3)$ and $W(x_3)$ can be expressed as follows [14,18–21]:

$$U(x_3)=\sum_{m=0}^{\infty} p_m^1Q_m(x_3),\quad V(x_3)=\sum_{m=0}^{\infty} p_m^2Q_m(x_3),\quad W(x_3)=\sum_{m=0}^{\infty} p_m^3Q_m(x_3) \tag{8}$$

Here, $p_m^i (i=1,2,3)$ are the expansion coefficients and

$$Q_m(x_3)=\sqrt{\frac{2m+1}{h_N}}P_m\left(\frac{2x_3}{h_N}-1\right)$$

where P_m is the mth Legendre polynomial. Theoretically, m runs from 0 to ∞. In practice, the order of the expansion in Eq.

(8) can be truncated to some finite value $m=M$ because the solution converges within a finite number of terms, when the higher order terms are effectively negligible.

Multiplying Eqs. (7a), (7b) and (7c) by $Q_j(x_3)$ with j running from 0 to M, integrating over x_3 from 0 to h_N, and making use of the orthogonality of the polynomials $Q_m(x_3)$ gives the following equations:

$$\begin{aligned}(A_{11}^{j,m}+\omega^2 M_m^j)p_m^1+A_{12}^{j,m}p_m^2+A_{13}^{j,m}p_m^3=0\\ A_{21}^{j,m}p_m^1+(A_{22}^{j,m}+\omega^2 M_m^j)p_m^2+A_{23}^{j,m}p_m^3=0\\ A_{31}^{j,m}p_m^1+A_{32}^{j,m}p_m^2+(A_{33}^{j,m}+\omega^2 M_m^j)p_m^3=0\end{aligned} \tag{9}$$

where summation over the repeated index m is implied with m ranging from 0 to M. The factors $A_{\alpha\beta}^{j,m}(\alpha,\beta=1,2,3)$ and M_m^j are the matrix elements, which are evaluated in the Appendix.

The non-zero solutions of Eq. (9) can only exist when the determinant of the coefficients of $p_m^i(i=1,2,3)$ equals zero, which yields

$$F(k,\omega)=\begin{vmatrix}A_{11}^{j,m}+\omega^2 M_m^j & A_{12}^{j,m} & A_{13}^{j,m}\\ A_{21}^{j,m} & A_{22}^{j,m}+\omega^2 M_m^j & A_{23}^{j,m}\\ A_{31}^{j,m} & A_{32}^{j,m} & A_{33}^{j,m}+\omega^2 M_m^j\end{vmatrix}=0 \tag{10}$$

Hence, the dispersion curves of coupled Lamb waves in a multilayered arbitrary anisotropic plate can be obtained by numerically solving Eq. (10). The solution of the dispersion equation can be reduced to an eigenvalue problem, which means Eq. (10) can be rewritten as

$$\begin{pmatrix}A_{11}^{j,m} & A_{12}^{j,m} & A_{13}^{j,m}\\ A_{21}^{j,m} & A_{22}^{j,m} & A_{23}^{j,m}\\ A_{31}^{j,m} & A_{32}^{j,m} & A_{33}^{j,m}\end{pmatrix}\begin{pmatrix}p_m^1\\ p_m^2\\ p_m^3\end{pmatrix}=\omega^2 M_m^j\begin{pmatrix}p_m^1\\ p_m^2\\ p_m^3\end{pmatrix} \tag{11}$$

The solutions to be accepted are only those eigenmodes for which convergence is obtained as M is increased [14–16]. We identify the converged solutions as the available eigenvalues when a further increase in matrix dimensionality does not lead to an obvious change of the eigenvalue. In this paper, the computer programs are written by using Mathematica software.

3. Numerical results

3.1. Validation of the approach by comparison with available data

Based on the formulations above, the relevant computer programs were explored for numerical calculation of the dispersion curves of coupled Lamb waves in multilayered anisotropic laminates. To check the validity of the formulations and programs, our approach was first implemented on a bi-layered isotropic plate. The plate is composed of an aluminum lamina (measuring 1 mm in thickness) and a brass lamina (measuring 1 mm in thickness). Their elastic constants are shown in Table 1. Then, the approach was further applied to a unidirectional fiber reinforced laminate, which is made of the graphite–epoxy composite material designated T300/914. The two component layers of the laminate are of the identical thickness 0.6 mm with the layering sequence [90°/0°]. The material properties of T300/914 at the fiber orientation angle 0° are listed in Table 2. The elastic tensors of the lamina at the fiber orientation angle 90° can be obtained by the transformation described in Section 3.2.1. The calculated results of two cases are shown in Fig. 2 for comparison with the available results obtained from the commercial software "Disperse" [8,26]. From Fig. 2, it can be observed that our solutions agree well with those calculated by "Disperse." In the two cases presented in this section, the truncated values are equal to 11 and 10, respectively.

3.2. Implementation of the approach for multilayered anisotropic composite laminates

A significant amount of work concerning the modeling of wave excitation, the analysis of simulation predictions, the characterization of material properties, the identification of structural defects, etc. has been reported by many researchers [27–34]. In the following section, the Legendre polynomial approach is used to analyze the propagation of coupled Lamb waves in multilayered anisotropic composite laminates because the validity of the method has been verified in the earlier section.

Table 1
The material properties of the bi-layered isotropic plate.

Property	c_{11} (GPa)	c_{13} (GPa)	c_{33} (GPa)	c_{55} (GPa)	ρ (g/cm^3)
Aluminum	107.8	54.94	107.8	26.45	2.7
Brass	162.6	81.3	162.6	40.7	8.4

Table 2
The material properties of the unidirectional fiber reinforced lamina T300/914.

c_{11} (GPa)	c_{12} (GPa)	c_{13} (GPa)	c_{22} (GPa)	c_{23} (GPa)
143.8	6.2	6.2	13.3	6.5
c_{33} (GPa)	c_{44} (GPa)	c_{55} (GPa)	c_{66} (GPa)	ρ (g/cm^3)
13.3	3.6	5.7	5.7	1.56

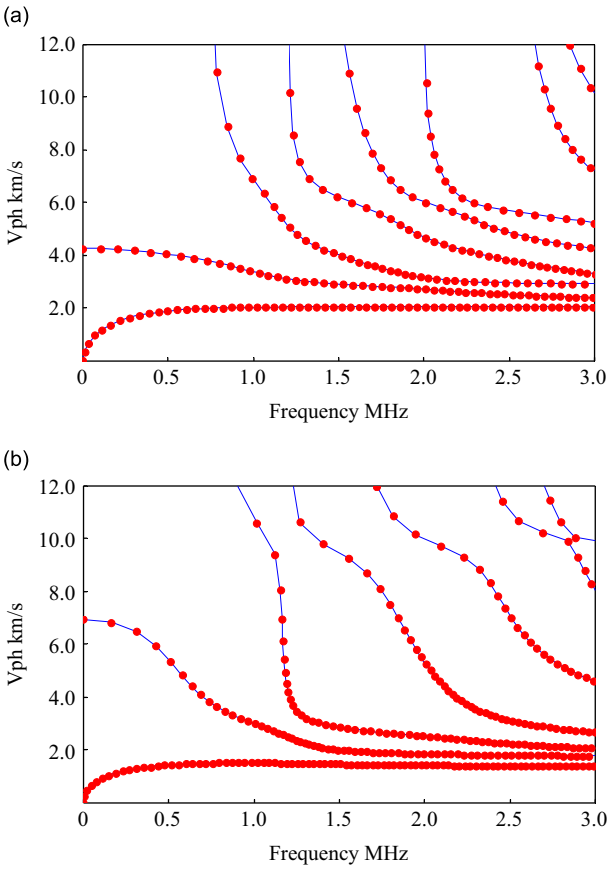

Fig. 2. Comparisons of the phase velocity dispersion curves for a bi-layered plate calculated by the author's programs (the red dotted line) with the available results of (a) an aluminum–brass bi-layered plate and (b) a 2-ply [90°/0°] composite laminate, obtained from "Disperse" software (the blue solid line). (For interpretation of the references to color in this figure legend, the reader is referred to the web version of this article.).

3.2.1. The effect of fiber orientation

In this section, we continue to use the unidirectional fiber reinforced composite material T300/914, specifically with respect to the effect of fiber orientation on the dispersion behavior of coupled Lamb wave propagation in multilayered anisotropic media. The material properties of T300/914 are given in Table 2. Each individual layer of the laminates is essentially made of the same composite material but with different orientation angles. Hence, the local reference coordinates $o{-}x_1' x_2' x_3'$ are established to denote the material properties of each lamina. To characterize the propagation of coupled Lamb waves, the elastic constants of every component layer in local reference coordinates must first be transformed into the effective quantities of the global coordinates $o{-}x_1 x_2 x_3$. As described in Fig. 3, the corresponding spatial coordinate systems indicate the relationship between the local reference coordinates and the global Cartesian coordinates.

For unidirectional fiber reinforced composite laminates, the transformation of the elastic tensors from the local reference coordinates to the global coordinates can be achieved using a tensor rotation process, formulated by Eq. (11), where β_{ij} indicates the cosine of the intersection angle ϕ between the x_i'-axis and x_j-axis $(i,j=1,2,3)$ [25]. Note that the value of the

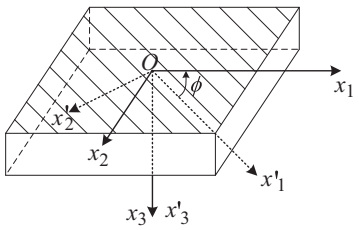

Fig. 3. The spatial coordinate systems with the dotted line representing the local reference coordinates and the solid line representing the global coordinates for a component layer.

intersection angle ϕ is positive when the rotation is in the counterclockwise direction.

$$c_{mnop} = \beta_{mi}\beta_{nj}\beta_{ok}\beta_{pl}c_{ijkl}' \tag{11}$$

To investigate the effect of fiber orientation, seven cases of tri-layer laminates are calculated with different layer sequences when the truncated value M is equal to 8. More specifically, the fiber orientations of the top and bottom layers are parallel in the x_1-axis direction and are unaltered as the orientation angle ϕ of the middle layer varies from 0° to 90° in increments of 15°. The total thickness of the laminates is 0.9 mm, which means every component layer occupies a region with a thickness of 0.3 mm. The calculated phase velocity dispersion curves of Lamb waves are shown in Fig. 4. Rigorously speaking, pure shear horizontal (SH) modes only exist in the principal direction. The distinction between the types of wave modes is somewhat artificial in a composite because three types of wave modes are generally coupled [35,36]. Conventionally, the symmetric (or extensional) and anti-symmetric (or flexural) Lamb wave modes can be denoted by S_n and A_n ($n = 0, 1, 2, 3\ldots$), respectively. The symmetric and anti-symmetric SH waves can be denoted by SH_n with even and odd subscripts of n. Here, we extend this concept and designate one wave mode type as a symmetric mode by symbols qS_n (quasi-extensional) and qSH_n (quasi-horizontal shear), if the dominant component of the polarization vector is along the propagation direction or is parallel to the plane of the plate. Likewise, the symbols qA_n (quasi-flexural) and qSH_{2n-1} (quasi-shear horizontal) are employed to indicate the anti-symmetric types. For the case of notation, in this paper, the prefix quasi is omitted unless stated otherwise. In Figs. 4(a) and (g), the phase velocity dispersion curves of SH_n modes are also incorporated because of the necessity of investigation, in which the waves actually propagate in the principal direction.

From Fig. 4, it can be observed that all Lamb wave modes can be classified into two categories. One category has no cut-off frequency in the low frequency range, while the other does. We mark the first category as the fundamental modes (S_0, A_0 and SH_0 modes) and the other as the high order modes. With the variation of fiber orientation in the middle layer, the shapes and positions of all of the curves are gradually shifted. For the high order modes, some branches, located within a certain frequency range over approximately 1.5–2 MHz and 2.5–3 MHz, appear to intersect each other when the Lamb waves propagate in the 0° principal direction. As the fiber orientation angle of the middle lamina increases, the branches begin to separate, which implies that the Lamb waves no longer propagate in the principal direction. Nevertheless, intersection occurs again when the fiber orientation angle of the middle lamina approaches 90° in the principal direction. This phenomenon reflects the effect of coupling on the propagation of higher order modes in composite laminates. In practice, due to the characteristics of serious dispersion, high attenuation and complex excitation, the higher order modes are rarely used for the inspection of defects. In contrast, the fundamental modes of Lamb waves are more often considered and selected for inspecting the damage incurred by multilayered laminates, which are attenuated less and are more easily identified [37–40]. Next, the fundamental modes are considered more closely, and a series of analyses on these modes is discussed in more depth.

With respect to the fundamental modes, it should be noted that there are some obvious non-dispersive segments over the low frequency range, especially beneath the first cut-off frequency. As the orientation angle ϕ of the middle layer increases, the maximum value of the phase velocity in the low frequency range decreases abruptly in allusion to the S_0 mode. However, for the SH_0 mode, the variation trend is distinctly different, increasing at first and then decreasing subsequently. If only the absolute magnitude of the velocity variation is considered, the variation of the S_0 mode is significantly larger than that of the SH_0 mode. This implies that the S_0 mode can be more sensitive to the variation of material properties and may be more suitable for use in the inspection and evaluation of anisotropic layered structures. Likewise, it can be observed that there are no evident changes for the A_0 mode in terms of the maximum value of the phase velocity at relevant low frequencies, as shown in Fig. 4.

To observe further the effect of fiber orientation on the fundamental modes, we select one arbitrary point located on the x_1-axis and theoretically predict the velocity variation at the frequency of 260 kHz when the orientation angle of the middle lamina changes. From Fig. 5, it is evident that the distributions of the phase velocity and group velocity are very consistent with respect to shape. Both of them are symmetric about the x_1-axis and x_3-axis, which reflects the symmetrical properties of the composite laminates. As the orientation angle ϕ of the middle lamina is varied from 0° through 90°, the predicted velocity values decrease monotonously for the S_0 mode and the A_0 mode. However, for the SH_0 mode, its velocity value

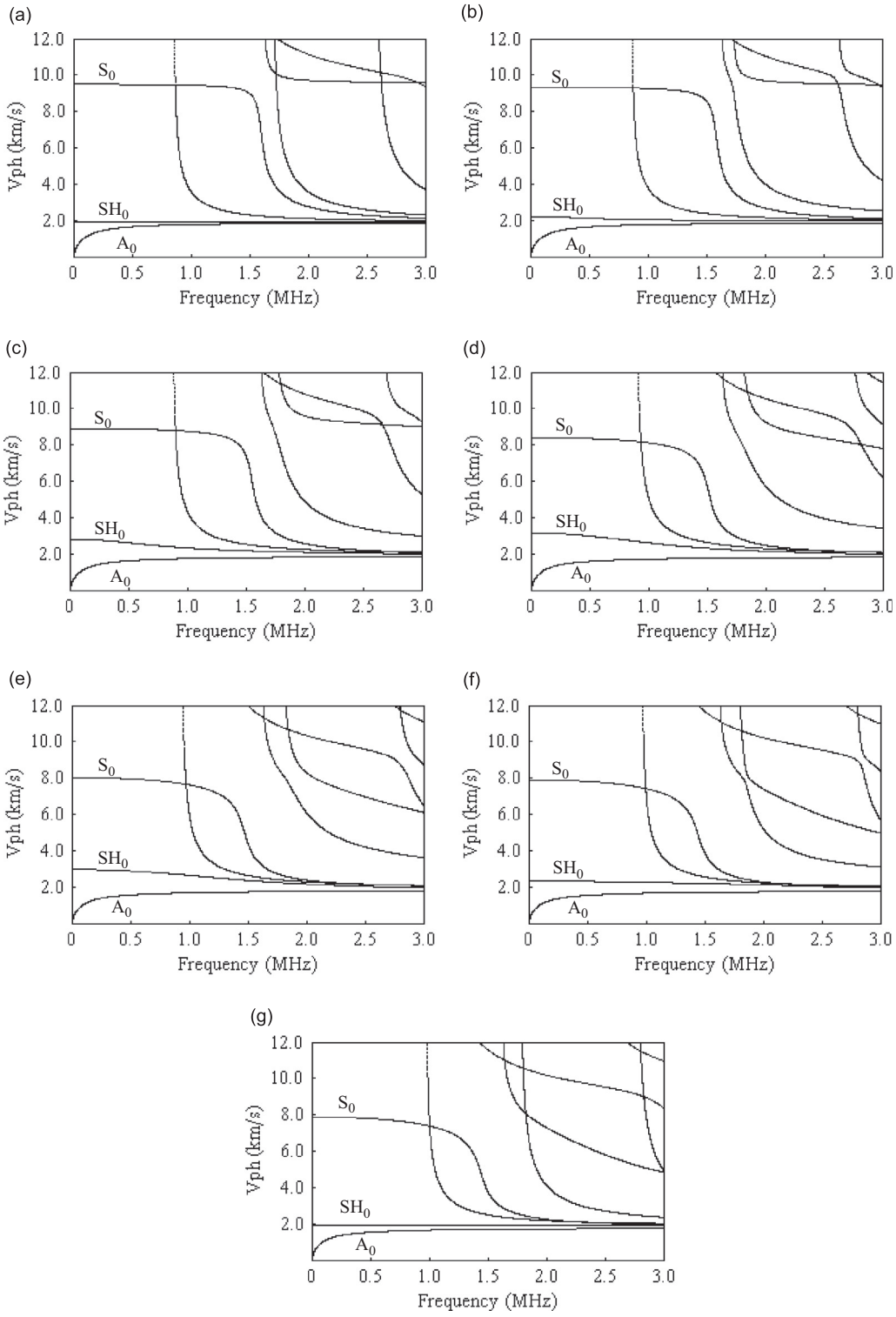

Fig. 4. The phase velocity dispersion curves of Lamb waves with different fiber orientations in the middle layer. (a) [0°/0°/0°] (b) [0°/15°/0°] (c) [0°/30°/0°] (d) [0°/45°/0°] (e) [0°/60°/0°] (f) [0°/75°/0°] (g) [0°/90°/0°].

increases first and subsequently decreases during this process. The fluctuation of amplitudes for both the S_0 mode and SH_0 mode are more significant than that of the A_0 mode.

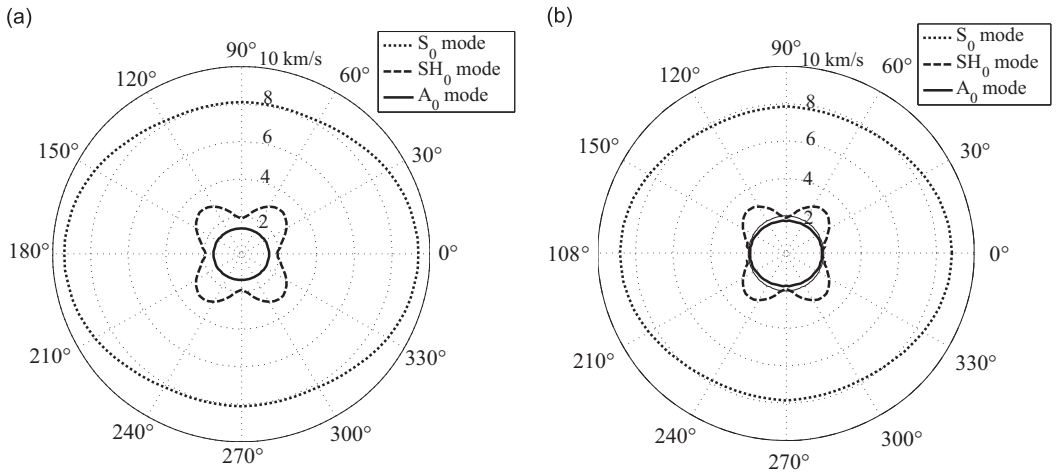

Fig. 5. The effect of fiber orientation in the middle layer on (a) the phase velocity and (b) group velocity of Lamb waves propagating along the x_1-axis direction at 260 kHz.

As shown in Fig. 5, the maximum values of group velocity are approximately 8809.00 m/s for the S_0 mode and 1919.64 m/s for the A_0 mode when the angle of the fiber orientation in the middle lamina coincides with the 0° principal direction. Likewise, the minimum group velocity values for the S_0 mode and the A_0 mode are 7865.84 m/s and 1729.9 m/s, respectively, when the orientation angle is along another 90° principal direction. Here, the concept of relative change rate can be used to evaluate the sensitivity of different modes to the fiber orientation of the middle layer. Through calculation, the relative change rates of the S_0 mode and the A_0 mode are 10.71 percent and 9.88 percent, respectively, in terms of the group velocity. It is obvious that these two values are approximately comparative, implying a similar sensitivity to the fiber orientation of the middle layer for the S_0 mode and the A_0 mode. This point is distinct relative to that observed from Fig. 4, where the absolute amplitude of the change of the S_0 mode is larger than that of the A_0 mode. The group velocity of the SH_0 mode approaches a maximum value of 3045.3 m/s when the fiber orientation is approximately along the 50° direction. Additionally, the minimum value of 1911.5 m/s can be obtained from the figure, and the relative change rate can be calculated as 37.23 percent. Comparing the S_0 mode with the A_0 mode, it is clear that the SH_0 mode is more sensitive to the fiber orientation in the middle layer, from the perspective of the relative change rate.

3.2.2. The displacement and stress distributions

In this section, the displacement and stress distributions of coupled Lamb wave modes in a tri-layer structure are investigated. Fig. 6, Fig. 7 and Fig. 8 show the displacement and stress distributions of the A_0 mode, SH_0 mode and S_0 mode, respectively, at different layering sequences. From the displacement distributions shown in these figures, it can be observed that particle vibration occurs in all three directions for coupled Lamb waves, which is different from that in the uncoupled situation. From Fig. 6, it can be observed that the normal displacement u_3 is symmetric about the central plane of the laminates for the A_0 mode, while its in-plane displacement u_1 and perpendicular displacement u_2 appear as asymmetric phenomena. The vibrational magnitude of the normal displacement u_3 is significantly larger than that of in-plane displacement u_1 and perpendicular displacement u_2, which means particle motion is mainly toward the x_3-axis direction and not the x_1-axis direction or x_2-axis direction. Additionally, it can be observed that there are no significant influences on the displacement distribution of the A_0 mode as the fiber orientation of the middle layer changes. However, for the stress distributions of the A_0 mode, the in-plane stress σ_{11} is predominant and mainly is distributed throughout the surface of the tri-layer laminates. The in-plane stress σ_{11} is asymmetric about the central plane of the laminates, but the normal stress σ_{33} and the shear stress σ_{31} appear oppositely. As the angle of the fiber orientation in the middle layer increases, the slope of the in-plane stress curve gradually becomes shallower in the through-thickness position from the approximate distance 0.3 mm to 0.6 mm. This phenomenon reflects the declining stiffness coefficients along the x_1-axis direction of the composite laminates.

Form Fig. 7, it can be observed that changing the angle of the fiber orientation ϕ has no significant influence on the displacement wave structure of the SH_0 mode, which is a similar finding to the performance of the A_0 mode. The direction of particle motion is mainly polarized in the horizontal x_2-axis direction, with minimal vibration in the other two directions. With respect to the stress distributions of the SH_0 mode, the curve of the in-plane stress σ_{11} is convex in shape, and abrupt increases and decreases occur in the curves at the through-thickness position of two interfaces. The distinct differences in the material properties on the respective sides of the interface are responsible for this phenomenon. As the angle of fiber orientation ϕ approaches 45°, the in-plane stress σ_{11} changes very little. When the orientation angle is larger than 45°, the in-plane stress σ_{11} decreases significantly. Compared with the stress polarization of the A_0 mode, the stress distribution of

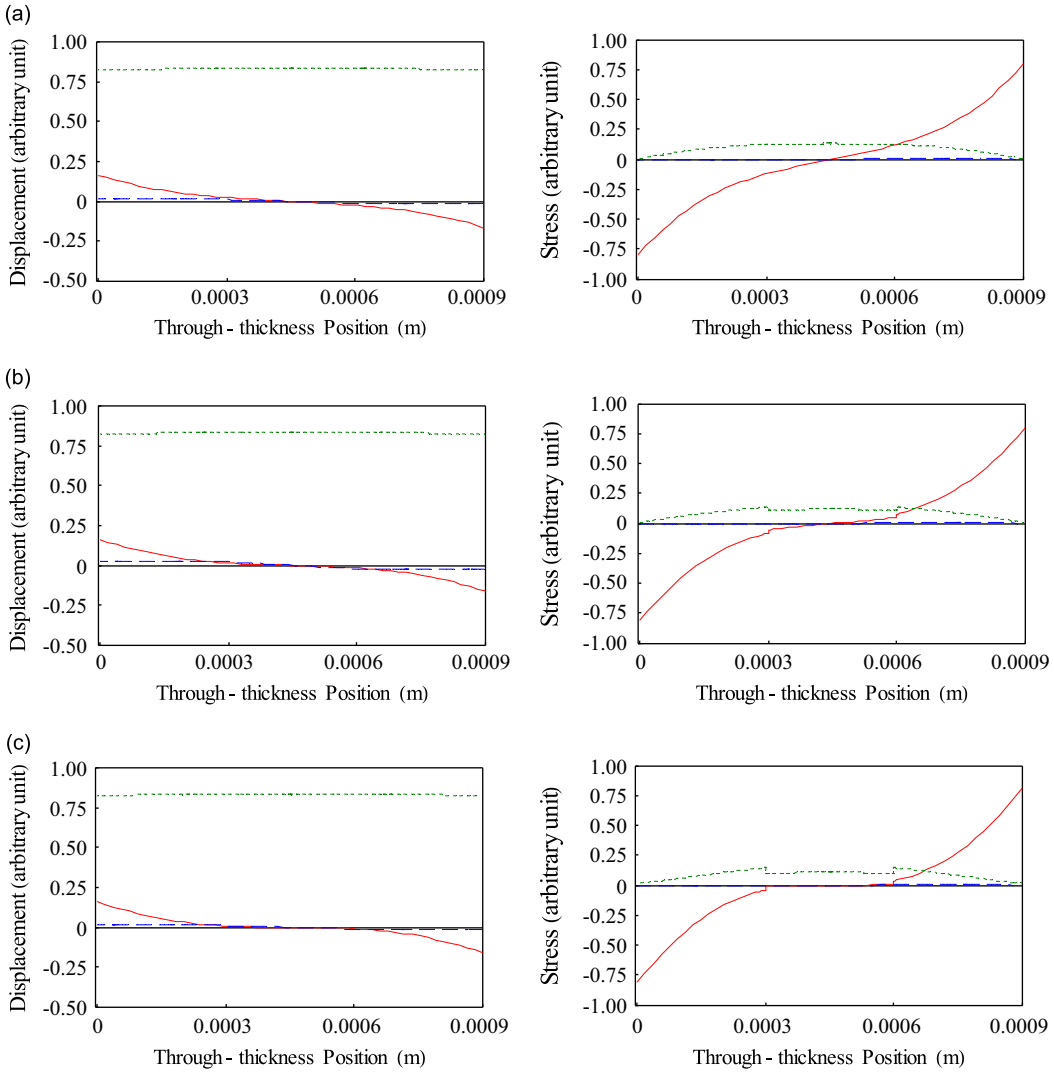

Fig. 6. The displacement and stress distributions of the A_0 mode at 260 kHz with different layering sequences (a) [0°/15°/0°], (b) [0°/45°/0°] and (c) [0°/75°/0°]. In the displacement distributions, the red solid line, blue dashed line and green dotted line represent the in-plane displacement u_1, perpendicular displacement u_2 and normal displacement u_3, respectively. In the stress distributions, the red solid line, blue dashed line and green dotted line represent the in-plane stress σ_{11}, normal stress σ_{33} and shear stress σ_{31}, respectively. (For interpretation of the references to color in this figure legend, the reader is referred to the web version of this article.).

the SH_0 mode is significantly smaller. Although the phase velocity feature of the SH_0 mode is more sensitive to the fiber orientation in the former discussion, the complex excitation result will create difficultly in the application of this model to the non-destructive testing and evaluation of the composite laminates; this difficulty is observed because the SH_0 mode is always coupled with other Lamb wave modes. Further, the stress value of the SH_0 mode is even smaller than the values of the A_0 and S_0 modes.

For the S_0 mode, a similar conclusion can be drawn regarding the analysis of the displacement distributions presented in Fig. 8. That is, increasing the fiber orientation angle has minimal influence on the displacement distribution of the S_0 mode. With respect to the stress distributions, as the angle of the fiber orientation is increased, the value of the in-plane stress σ_{11} within the middle layer decreases gradually. However, the in-plane stresses in the top and bottom layers vary minimally during this process. Through the previous analysis, we can see that both the A_0 and S_0 modes can be used to test and evaluate the structural integrity of anisotropic composite laminates. The effect of fiber orientation on the in-plane stress distribution is more significant for the S_0 mode than the A_0 mode. However, the wavelength of the A_0 mode is significantly shorter than that of the S_0 mode because the phase velocity of the A_0 mode is always smaller than that of the S_0 mode in the low frequency range, which means that the resolution of the A_0 mode will be higher during evaluation. Due to the effect of coupling, it is difficult to apply the SH_0 mode in the non-destructive testing and evaluation of anisotropic laminates.

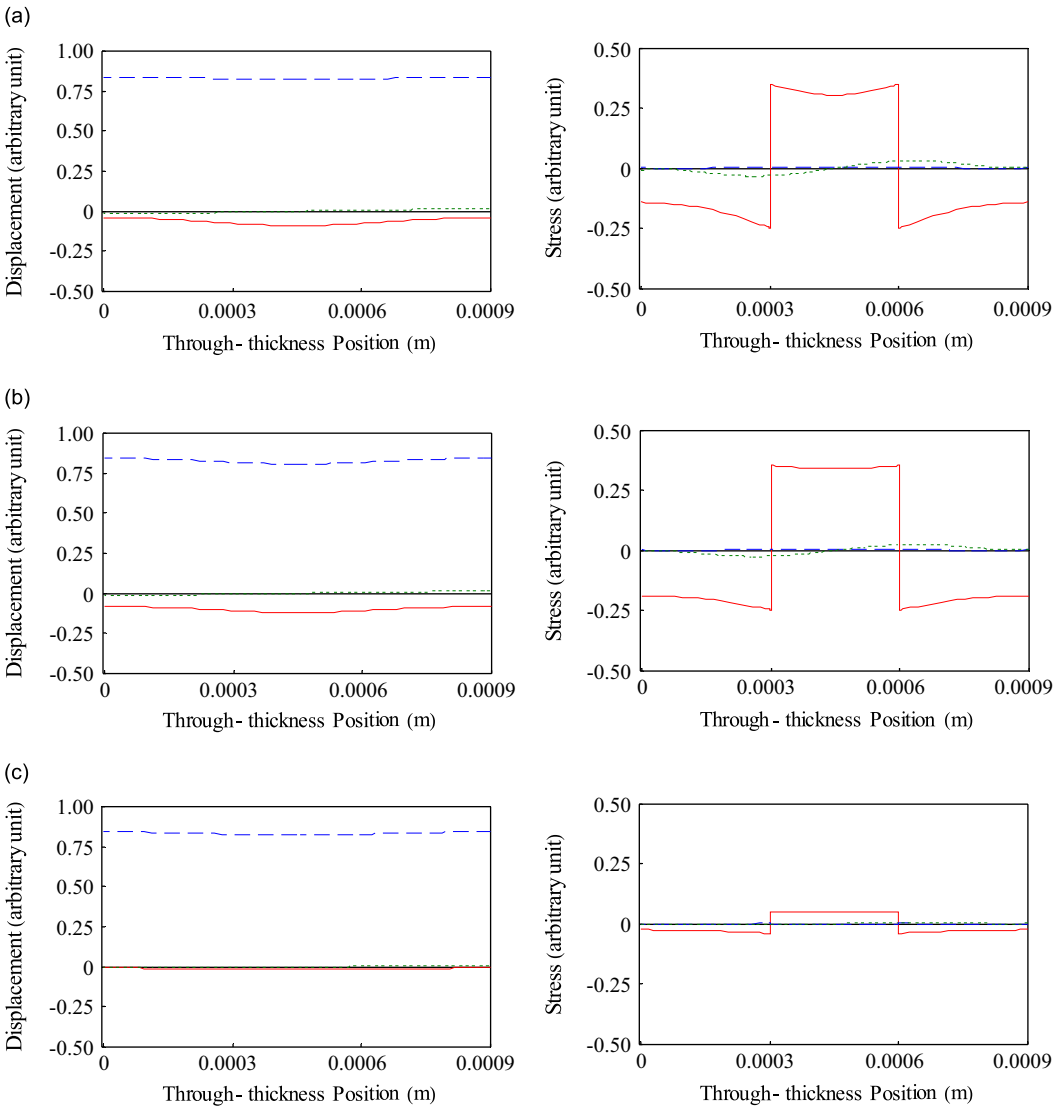

Fig. 7. The displacement and stress distributions of the SH_0 mode at 260 kHz with different layering sequences (a) [0°/15°/0°], (b) [0°/45°/0°] and (c) [0°/75°/0°]. In the displacement distributions, the red solid line, blue dashed line and green dotted line represent the in-plane displacement u_1, perpendicular displacement u_2 and normal displacement u_3, respectively. In the stress distributions, the red solid line, blue dashed line and green dotted line represent the in-plane stress σ_{11}, normal stress σ_{33} and shear stress σ_{31}, respectively. (For interpretation of the references to color in this figure legend, the reader is referred to the web version of this article.).

4. Conclusion

In the context of linear three-dimensional elasticity theory, the Legendre orthogonal polynomial approach is used to characterize the propagation of coupled Lamb waves in multilayered arbitrary anisotropic composite laminates. The dispersion curves, displacement and stress distributions of coupled Lamb waves in multilayered anisotropic laminates with different layering sequences are calculated. Based on the results, the following summary of conclusions can be provided:

(a) Fiber orientation significantly influences the dispersion curves of the fundamental Lamb wave modes using coupled Lamb waves.
(b) The effects of fiber orientation on the phase velocity characteristics of the A_0 mode and S_0 mode are approximately similar and are smaller than that of the SH_0 mode.
(c) Changes in fiber orientation minimally influence the displacement distribution of the propagation of coupled Lamb waves in anisotropic composites.

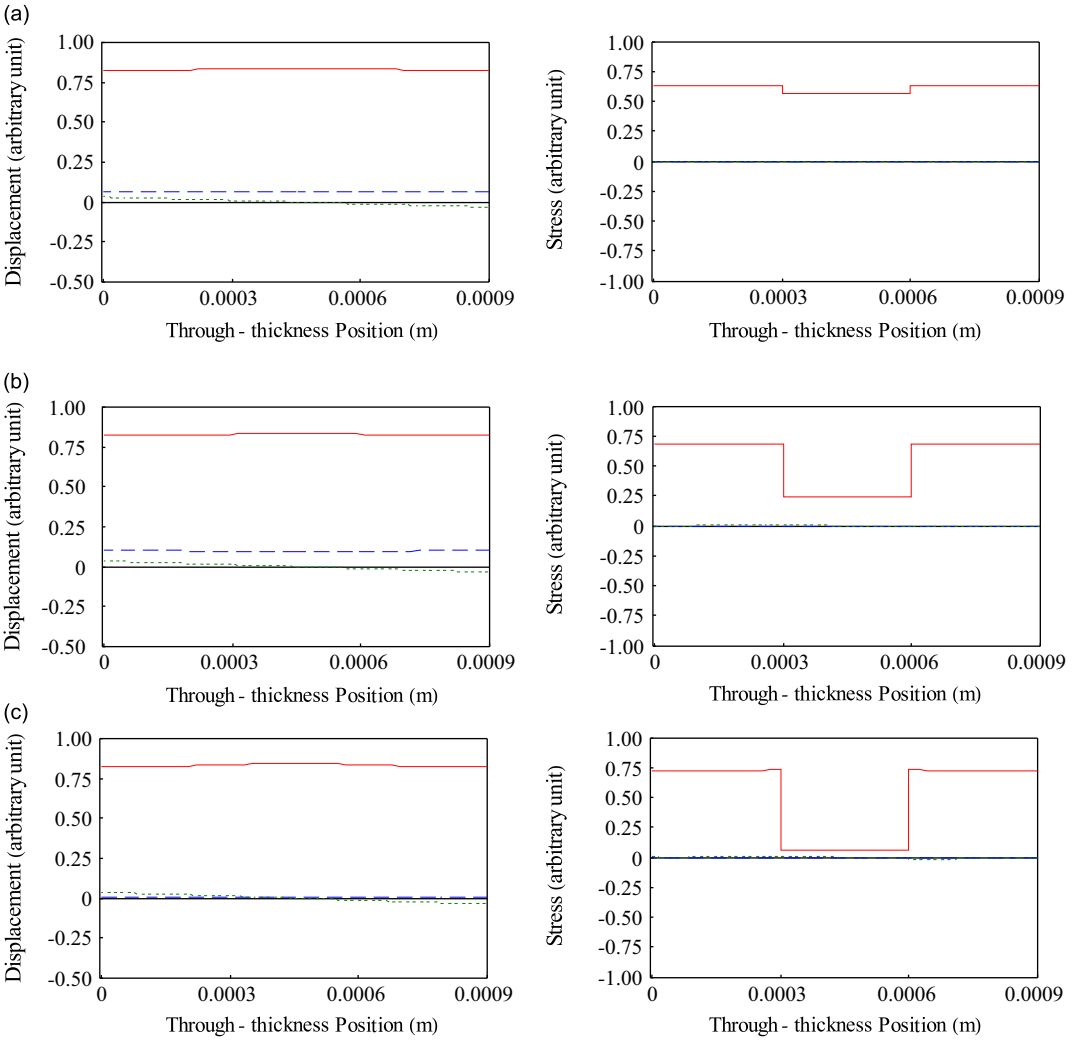

Fig. 8. The displacement and stress distributions of the S_0 mode at 260 kHz with different layering sequences (a) [0°/15°/0°], (b) [0°/45°/0°] and (c) [0°/75°/0°]. In the displacement distributions, the red solid line, blue dashed line and green dotted line represent the in-plane displacement u_1, perpendicular displacement u_2 and normal displacement u_3, respectively. In the stress distributions, the red solid line, blue dashed line and green dotted line represent the in-plane stress σ_{11}, normal stress σ_{33} and shear stress σ_{31}, respectively. (For interpretation of the references to color in this figure legend, the reader is referred to the web version of this article.).

(d) Due to the effect of coupling, it is difficult to apply the SH_0 mode in the evaluation of anisotropic laminates, while the A_0 mode and S_0 mode may be useful in this application.

Acknowledgments

This work was supported by the National Natural Science Foundation of China (Nos. 51235001, 11272021 and 50975006), the Beijing Natural Science Foundation (No. 1122007), the General Program of Science and Technology Development Project of the Beijing Municipal Commission of Education (No. KM201010005003) and the Beijing Nova Program (No. 2008A015).

Appendix

The matrix elements $A_{\alpha\beta}^{j,m}$ and M_m^j in Eq. (9) are:

$$A_{11}^{j,m} = c_{55}u(j,m,0,2)+(ik)2c_{15}u(j,m,0,1)+(ik)^2c_{11}u(j,m,0,0)+c_{55}K(j,m,0,1)+(ik)c_{15}K(j,m,0,0)$$

$$A_{12}^{j,m} = c_{45}u(j,m,0,2)+(ik)(c_{14}+c_{16})u(j,m,0,1)+(ik)^2c_{16}u(j,m,0,0)+c_{45}K(j,m,0,1)+(ik)c_{56}K(j,m,0,0)$$

$$A_{13}^{j,m} = c_{35}u(j,m,0,2)+(ik)(c_{13}+c_{55})u(j,m,0,1)+(ik)^2c_{15}u(j,m,0,0)+c_{35}K(j,m,0,1)+(ik)c_{55}K(j,m,0,0)$$

$$A_{21}^{j,m} = c_{45}u(j,m,0,2)+(ik)(c_{14}+c_{56})u(j,m,0,1)+(ik)^2c_{16}u(j,m,0,0)+c_{45}K(j,m,0,1)+(ik)c_{14}K(j,m,0,0)$$

$$A_{22}^{j,m} = c_{44}u(j,m,0,2)+(ik)2c_{46}u(j,m,0,1)+(ik)^2c_{66}u(j,m,0,0)+c_{44}K(j,m,0,1)+(ik)c_{46}K(j,m,0,0)$$

$$A_{23}^{j,m} = c_{34}u(j,m,0,2)+(ik)(c_{36}+c_{45})u(j,m,0,1)+(ik)^2c_{56}u(j,m,0,0)+c_{34}K(j,m,0,1)+(ik)c_{45}K(j,m,0,0)$$

$$A_{31}^{j,m} = c_{35}u(j,m,0,2)+(ik)(c_{13}+c_{55})u(j,m,0,1)+(ik)^2c_{15}u(j,m,0,0)+c_{35}K(j,m,0,1)+(ik)c_{13}K(j,m,0,0)$$

$$A_{32}^{j,m} = c_{34}u(j,m,0,2)+(ik)(c_{36}+c_{45})u(j,m,0,1)+(ik)^2c_{56}u(j,m,0,0)+c_{34}K(j,m,0,1)+(ik)c_{36}K(j,m,0,0)$$

$$A_{33}^{j,m} = c_{33}u(j,m,0,2)+(ik)2c_{35}u(j,m,0,1)+(ik)^2c_{55}u(j,m,0,0)+c_{33}K(j,m,0,1)+(ik)c_{35}K(j,m,0,0)$$

$$M_m^j = u(j,m,0,0)$$

$$u(j,m,n,l) = \int_a^b Q_j^*(x_3)\cdot {x_3}^n \cdot \frac{\partial^l Q_m(x_3)}{\partial {x_3}^l} dx_3$$

$$K(j,m,n,l) = \int_a^b Q_j^*(x_3)\cdot {x_3}^n \cdot \frac{\partial^l Q_m(x_3)}{\partial {x_3}^l} \frac{\partial[\pi(x_3-a)-\pi(x_3-b)]}{\partial x_3} dx_3$$

References

[1] A.H. Nayfeh, D.E. Chimenti, Elastic wave propagation in fluid-loaded multiaxial anisotropic media, *Journal of the Acoustical Society of America* 89 (1991) 542–549.
[2] A.H. Nayfeh., The general problem of elastic wave propagation in multilayered anisotropic media, *Journal of the Acoustical Society of America* 89 (1991) 1521–1531.
[3] A.H. Nayfeh, *Wave Propagation in Layered Anisotropic Media With Applications to Composites*, Elsevier, Amsterdam, 1995.
[4] B. Hosten, M. Castaings, Transfer matrix of multilayered absorbing and anisotropic media: measurements and simulations of ultrasonic wave propagation through composite materials, *Journal of the Acoustical Society of America* 94 (1993) 1488–1495.
[5] C. Potel, J.F. De Belleval, Propagation in an anisotropic periodically multilayered medium, *Journal of the Acoustical Society of America* 93 (1993) 2669–2677.
[6] J.A. Ogilvy., A model for the ultrasonic inspection of composite plates, *Ultrasonics* 33 (1995) 85–93.
[7] L. Knopoff., A matrix method for elastic wave problems, *Bulletin of the Seismological Society of America* 54 (1964) 431–438.
[8] M.J.S. Lowe, Matrix techniques for modeling ultrasonic waves in multilayered media, *IEEE Transactions on Ultrasonics, Ferroelectrics, and Frequency Control* 42 (1995) 525–542.
[9] B. Hosten, M. Castaings., FE modeling of Lamb mode diffraction by defects in anisotropic viscoelastic plates, *NDT & E International* 39 (2006) 195–204.
[10] C.T. Ng, M. Veidt, Scattering of the fundamental anti-symmetric Lamb wave at delaminations in composite laminates, *Journal of the Acoustical Society of America* 129 (2011) 1288–1296.
[11] H.M. Al-Qahtani, S.K. Datta, O.M. Mukdadi, Laser-generated thermoelastic waves in an anisotropic infinite plate: FEM analysis, *Journal of Thermal Stress* 28 (2005) 1099–1122.
[12] X.Y. Li, Z.K. Wang, S.H. Huang, Love waves in functionally graded piezoelectric materials, *International Journal of Solids and Structures* 41 (2004) 7309–7328.
[13] J. Liu, Z.K. Wang, The propagation behavior of Love waves in a functionally graded layered piezoelectric structure, *Smart Materials and Structures* 14 (2005) 137–146.
[14] J.E. Lefebvre, V. Zhang, J. Gazalet, T. Gryba, V. Sadaune, Acoustic wave propagation in continuous functionally graded plates: an extension of the Legendre polynomial approach, *IEEE Transactions on Ultrasonics, Ferroelectrics, and Frequency Control* 48 (2001) 1332–1339.
[15] L. Elmaimouni, J.E. Lefebvre, V. Zhang, T. Gryba., A polynomial approach to the analysis of guided waves in anisotropic cylinders of infinite length, *Wave Motion* 42 (2005) 177–189.
[16] L. Elmaimouni, J.E. Lefebvre, V. Zhang, T. Gryba, Guided waves in radially graded cylinders: a polynomial approach, *NDT&E International* 38 (2005) 344–363.
[17] Y. Kim, W.D. Hunt, Acoustic fields and velocities for surface-acoustic-wave propagation in multilayered structures: an extension of the Laguerre polynomial approach, *Journal of Applied Physics* 68 (1990) 4993–4997.
[18] B. Wu, J.G. Yu, C.F. He, Wave propagation in non-homogeneous magneto–electro-elastic plates, *Journal of Sound and Vibration* 317 (2008) 250–264.
[19] J.G. Yu, B. Wu, Circumferential wave in magneto–electro-elastic functionally graded cylindrical curved plates, *European Journal of Mechanics A/Solids* 28 (2009) 560–568.
[20] J.G. Yu, Q.J. Ma, Wave characteristics in magneto–electro-elastic functionally graded spherical curved plates, *Mechanics of Advanced Materials and Structures* 17 (2010) 287–301.
[21] J.G. Yu, F.E. Ratolojanahary, J.E. Lefebvre, Guided wave in functionally graded viscoelastic plates, *Composite Structures* 93 (2011) 2671–2677.
[22] M.V. Predoi, M. Castaings, B. Hosten, C. Bacon, Wave propagation along transversely periodic structures, *Journal of the Acoustical Society of America* 121 (2007) 1935–1944.
[23] O. Lenoir, L. Guénégou., The phase gradient method: application to the obtaining of the dispersion curves and the energy velocity of anisotropic plate modes, *ACTA Acustica United with Acustica* 95 (2009) 501–511.
[24] S. Banerjee, C.B. Pol., Theoretical modeling of guided wave propagation in a sandwich plate subjected to transient surface excitations, *International Journal of Solids and Structures* 49 (2012) 3233–3241.
[25] S.H. Rhee, J.K. Lee, J.J. Lee., The group velocity variation of Lamb wave in fiber reinforced composite plate, *Ultrasonics* 47 (2007) 55–63.
[26] D.O. Thompson, D.E. Chimenti, *Review of Progress in Quantitative Nondestructive Evaluation*, Plenum Press, New York, 1997.
[27] A. Velichko, P.D. Wilcox, Modeling the excitation of guided waves in generally anisotropic multilayered media, *Journal of the Acoustical Society of America* 121 (2007) 60–69.

[28] C.T. Ng, M. Veidt, L.R.F. Rose, C.H. Wang, Analytical and finite element prediction of Lamb wave scattering at delaminations in quasi-isotropic composite laminates, *Journal of Sound and Vibration* 331 (2012) 4870–4883.
[29] H. Gravenkamp, C.M. Song, J. Prager., A numerical approach for the computation of dispersion relations for plate structures using the scaled boundary finite element method, *Journal of Sound and Vibration* 331 (2012) 2543–2557.
[30] H.K. Peng, G. Meng, F.C. Li, Modeling of wave propagation in plate structures using three-dimensional spectral element method for damage detection, *Journal of Sound and Vibration* 320 (2009) 942–954.
[31] H. Kaczmarek, Lamb waves interaction with impact-induced damage in aircraft composite: use of the A_0 mode excited by air-coupled transducer, *Journal of Composite materials* 37 (2003) 217–232.
[32] O.I. Lobkis, D.E. Chimenti, H. Zhang, In-plane elastic property characterization in composite plates, *Journal of the Acoustical Society of America* 107 (2000) 1852–1858.
[33] J. Moll, C.P. Fritzen, Guided waves for autonomous online identification of structural defects under ambient temperature variations, *Journal of Sound and Vibration* 331 (2012) 4587–4597.
[34] R. Medina, A. Bayón, Elastic constants of a plate from impact-echo resonance and Rayleigh wave velocity, *Journal of Sound and Vibration* 329 (2010) 2114–2126.
[35] T.C.T. Ting, *Anisotropic Elasticity Theory and Applications*, Oxford University Press, New York, 1996.
[36] L. Wang, F.G. Yuan, Group velocity and characteristic wave curves of Lamb waves in composite: modeling and experiments, *Composite Science and Technology* 67 (2007) 1370–1384.
[37] E.A. Birt, Damage detection in carbon-fiber composite using ultrasonic Lamb waves, *Insight* 40 (1998) 335–339.
[38] P. Cawley., The rapid non-destructive inspection of large composite structures, *Composites* 25 (1994) 351–357.
[39] M.X. Deng, J. Yang, Characterization of elastic anisotropy of a solid plate using nonlinear Lamb wave approach, *Journal of Sound and Vibration* 308 (2007) 201–211.
[40] H. Sohn, G. Park, J.R. Wait, N.P. Limback, C.R. Farrar, Wavelet-based active sensing for delamination in composite structures, *Smart Materials and Structures* 13 (2004) 153–160.